Am J Cancer Res 2026;16(8):3359-3376
www.ajcr.us /ISSN:2156-6976/ajcr0173914

Original Article

Identification of differential miRNAs in serum exosomes and development of an integrated diagnostic model for early gastric cancer

Jianming Wei*, Puyu Luo*, Wen Yao, Dawei Di, Junfu Wang

*Department of General Surgery, The First Affiliated Hospital, Jiangxi Medical College, Nanchang University, Nanchang 330006, Jiangxi, China. *Equal contributors.*

Received May 9, 2026; Accepted June 30, 2026; Epub August 15, 2026; Published August 30, 2026

Abstract: Early detection of gastric cancer (GC) improves patient outcomes. However, conventional serum biomarkers show limited sensitivity in early disease stages. Circulating microRNAs (miRNAs) are remarkably stable in body fluids. These molecules have emerged as promising noninvasive biomarkers. In this study, we isolated serum-derived exosomes from healthy controls and GC patients. Transmission electron microscopy, nanoparticle tracking analysis, and Western blotting confirmed exosomal characteristics. Small RNA sequencing then established miRNA expression profiles to identify progression-associated molecules. We conducted bioinformatics analyses to explore their biological roles and validated candidate miRNAs using quantitative real-time PCR. Notably, miR-17-3p levels declined progressively during disease development. This expression level correlated significantly with tumor differentiation (P = 0.0324), TNM stage (P = 0.0100), and neural invasion (P = 0.0100). Combining miR-17-3p with conventional markers increased the area under the curve (AUC) from 0.7847 to 0.8472 for staging. These findings demonstrate that serum exosomal miR-17-3p is a promising biomarker for GC diagnosis and evaluation.

Keywords: Early-stage gastric cancer, small RNA sequencing, exosome, miR-17-3p, diagnostic model

Introduction

Gastric cancer (GC) remains a major global public health problem. Epidemiological data from 2022 rank GC fifth in global incidence. It follows breast, lung, colorectal, and prostate cancers. Concurrently, GC ranks fifth in global mortality [1, 2]. Recent projections indicate a 60% increase in new cases by 2040 [3]. Patient prognosis depends heavily on the disease stage at diagnosis. Most patients exhibit subtle early symptoms. Consequently, most patients are diagnosed at an advanced stage [4]. This late diagnosis narrows the therapeutic window. It also significantly elevates the risk of death. Enhanced early screening is therefore crucial to reduce the disease burden. Endoscopic biopsy remains the gold standard for GC diagnosis. However, this invasive procedure carries risk of trauma. The associated medical cost is also relatively high. These limitations hinder its adoption for large-scale population screening. Developing novel, non-invasive biomarkers is essential to improve early detection and patient outcomes.

Exosomes are lipid bilayer-enclosed extracellular vesicles. These structures typically range from 40 to 100 nm in size. They carry multiple bioactive components, including proteins, lipids, and various non-coding RNAs [5, 6]. Among these components, microRNAs (miRNAs) represent a prominent class of single-stranded non-coding RNAs. These endogenous molecules are approximately 17-24 nucleotides long. Mechanistically, miRNAs bind partially to the 3'-UTR of target messenger RNAs [7]. This interaction regulates post-transcriptional gene expression. It leads to translational repression or target mRNA degradation. By shuttling these functional cargoes, exosomes mediate intercellular communication. They modulate signaling pathways in both physiological and pathological contexts [8]. Furthermore, the lipid bilayer membrane protects encapsulated miRNAs. This protective barrier enhances miRNA stabili-

https://doi.org/10.62347/AOPT3512

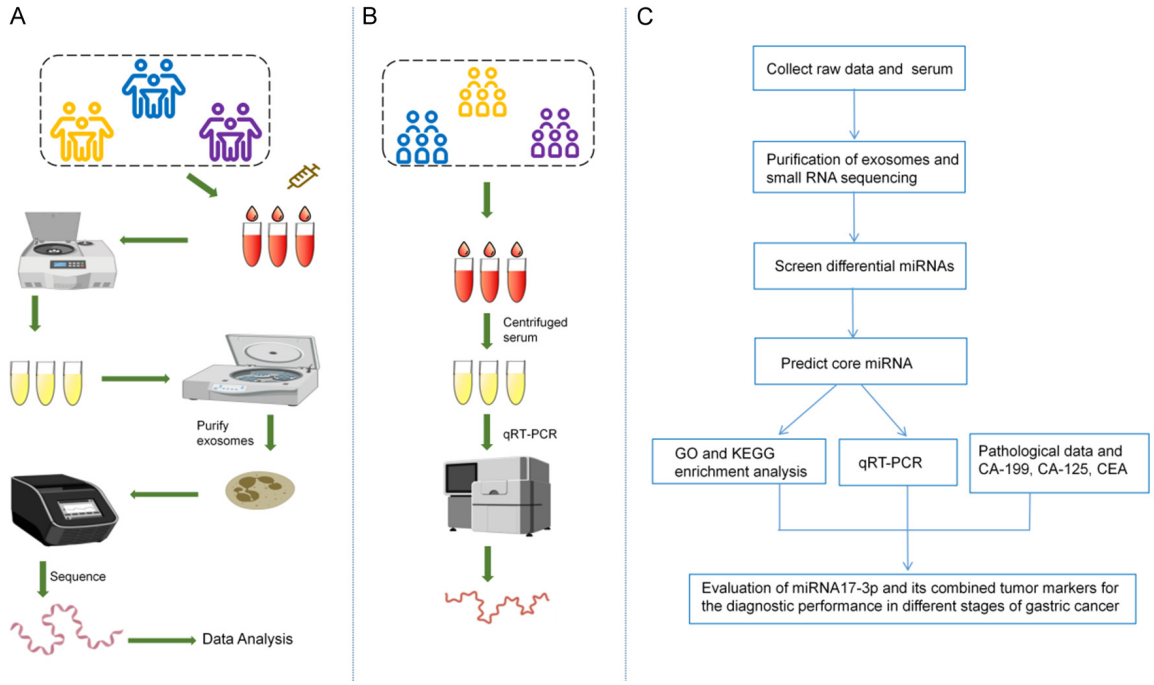

Figure 1. Flowchart. A. Small RNA high-throughput sequencing. B. qRT-PCR detection of core miRNA. C. Study design diagram. GO: Gene Ontology; KEGG: Kyoto Encyclopedia of Genes and Genomes; CA-199: carbohydrate antigen 199; CA-125: carbohydrate antigen 125; CEA: carcinoembryonic antigen.

ty in hostile bodily fluids [9]. In GC, exosomes deliver specific functional cargoes to the tumor microenvironment. These molecules directly influence cancer cell proliferation, invasion, and migration [10-12]. Prior research suggests a potential biomarker role for plasma exosomal miR-10b-5p and miR-101-3p in metastatic GC [13]. These specific miRNAs correlate with ovarian, liver, and lymph node metastases. However, the diagnostic utility of serum exosomal miRNAs for early-stage GC remains poorly understood.

This study profiled serum exosomal miRNA expression using small RNA high-throughput sequencing. We compared these profiles among healthy volunteers, early GC patients, and advanced GC patients. This analysis identified differentially expressed miRNAs between the study groups. We performed functional enrichment analyses to uncover molecules linked to GC progression. Quantitative real-time PCR subsequently validated the candidate miRNAs. Ultimately, this project evaluated the clinical value of serum exosomal miRNAs for early GC screening. The findings provide a scientific basis for non-invasive diagnostic systems. This approach may significantly improve early detection strategies for gastric cancer.

Materials and methods

Study subjects

This study was conducted in two distinct stages. From August 2024 to December 2025, we enrolled gastric cancer patients at the First Affiliated Hospital of Nanchang University. Healthy subjects were recruited during the same period as controls. In the initial stage, we selected three healthy individuals (Group N). We also included three early-stage patients (Group T1, TNM 0-I) and three advanced-stage patients (Group T2, TNM II-III). Small RNA high-throughput sequencing analyzed serum specimens from these nine participants (**Figure 1A**). For the validation stage, the cohort comprised 24 gastric cancer patients. This group included 12 early-stage (Group T1) and 12 advanced-stage (Group T2) cases. Additionally, we enrolled 12 healthy controls (Group N). Quantitative real-time PCR (qRT-PCR) analyzed all second-stage serum samples (**Figure 1B**). Preoperative gastroscopy and pathological biopsy confirmed gastric cancer in all patients. We excluded individuals with distant metastasis detected before or during surgery. Patients receiving prior neoadjuvant chemotherapy or radiotherapy were also excluded. Clinicians

collected comprehensive clinicopathological data for all patients. These parameters included sex, age, tumor diameter, and differentiation degree. Lymph node status, nerve invasion, vascular emboli, and TNM stage were also recorded. **Figure 1C** summarizes the overall study workflow. This study was approved by the Ethics Committee of the First Affiliated Hospital of Nanchang University ((2024) CDYFYYLK (07-043)).

Serum separation and purification

We obtained 25 mL of peripheral venous blood from each participant. Centrifugation at 3000×g for 15 minutes separated the serum fraction. We carefully transferred the upper layer into a clean tube. A second centrifugation at 12000×g for 30 minutes eliminated residual cells and debris. This process yielded a clear supernatant. Finally, we stored the purified serum.

Purification of serum exosomes

We thoroughly mixed a 5 mL serum aliquot with XBP buffer. This mixture was then loaded onto an exoEasy spin column. Centrifugation at 5000×g for 1 minute followed, and we discarded the flow-through. We added XWP buffer to the column. A second centrifugation at 5000×g for 5 minutes washed the membrane. After discarding the waste solution, we transferred the column into a clean collection tube.

Measurement of exosome particle size and observation by transmission electron microscopy

We slowly injected the diluted exosome suspension into a nanoparticle tracking analyzer. The instrument automatically tracked the Brownian motion of the nanoparticles. This system output data regarding exosome size distribution and concentration. For electron microscopy, we pipetted 10 µL of the exosome sample onto a copper grid. The droplet stood at room temperature for 5 minutes. Next, dry filter paper carefully absorbed the excess liquid. We applied one drop of 2% uranyl acetate to the grid for negative staining. After 1 minute, filter paper blotted away the residual staining solution. The grid dried completely at room temperature. We observed the morphological characteristics of the exosomes using transmission electron microscopy.

Western blot

We separated equal amounts of protein from each group using 10% SDS-PAGE. A wet transfer system then moved the resolved proteins onto PVDF membranes (Millipore, USA). Next, we blocked the membranes at room temperature for 1.5 hours. This step utilized 5% non-fat milk prepared in Tris-buffered saline. Primary antibodies against CD9 and TSG101 (1:500; Abcam, UK) incubated with the membranes overnight. After three 8-minute washes, we introduced a horseradish peroxidase-conjugated goat anti-rabbit IgG secondary antibody (1:1000; CST, USA). This incubation lasted for 1 hour. We repeated the 8-minute wash step three times. An enhanced chemiluminescence (ECL) substrate (Beyotime, China) was applied evenly to the membranes. A chemiluminescence imaging system finally detected target protein expression.

Extraction of serum exosomal miRNAs

We homogenized an aliquot of purified serum exosomes in 700 µL QIAzol lysis reagent. Next, we introduced 140 µL of nuclease-free chloroform. The mixture was inverted for 15 seconds and incubated for 3 minutes. Centrifugation at 12000×g for 15 minutes at 4°C separated the phases. We carefully transferred the upper aqueous supernatant into a clean tube. Mixing followed with a 1.5-fold volume of ethanol. We then loaded the sample onto an RNeasy MinElute spin column. After centrifugation at 10000×g for 15 seconds, we discarded the eluate. We rinsed the column with 700 µL RWT buffer under identical centrifugation parameters. The column was subsequently moved to a fresh collection tube. To recover RNA, we added 15 µL of pre-warmed DEPC-treated water. A 2-minute incubation followed. A final centrifugation step at 12000×g for 1 minute eluted the RNA. UV spectrophotometry ultimately evaluated total RNA quality and concentration.

Construction of small RNA libraries

After total RNA extraction, agarose gel electrophoresis isolated small RNA fragments. We selected molecules ranging from 18 to 30 nucleotides through gel recovery. Then we sequentially ligated specific adapters to the 3' and 5' termini. Reverse transcription and sub-

Table 1. The primer sequences of qRT-PCR

Gene	Primer	Sequence (5'-3')
U6	Forward	CGCTTCGGCAGCACATATAC
	Reverse	AAATATGGAACGCTTCACGA
miR-17-3p	Loop primer	GTCGTATCCAGTGCAGGGTCCGAGGTATTCGCACTGGATACGACCTACAAGT
	F primer	TGCGCACTGCAGTGAAGGCACT

sequent PCR amplification followed to process the ligation products. Agarose gel electrophoresis then separated the resulting PCR products. From the gel, we excised and purified fragments of approximately 140 bp. This final purification step successfully generated the small RNA libraries.

Visualization analysis of miRNAs

We performed Principal Component Analysis (PCA) on the Transcripts Per Million (TPM) expression matrix. This analysis utilized the stats package in R. The resulting plots visualized overall expression distributions and intergroup separation trends. The edge R software identified differentially expressed miRNAs through pairwise comparisons. We applied strict thresholds of $|\log_2(\text{fold change})| \geq 1$ and an adjusted *P*-value < 0.05. The ggplot2 package in R generated scatter plots to depict intergroup expression differences. Finally, we constructed a heatmap using the pheatmap package. This visualization displayed the specific expression patterns of differentially expressed miRNAs across individual samples.

Gene ontology (GO) and Kyoto encyclopedia of genes and genomes (KEGG) enrichment analysis, and target gene prediction

Systematic enrichment analysis was performed for each expression module and for differentially expressed miRNAs using the cluster Profiler R package. We annotated miRNA target genes through Gene Ontology analysis. KEGG pathway analysis was further used to explore signaling pathways associated with these miRNAs (Enrichment significance was adjusted *P* value < 0.05). Results from GO and KEGG analyses were visualized using the ggplot2 package in the form of bubble charts and bar plots. Target gene prediction was carried out by combining outputs from TargetScan (v7.0), miRanda (v3.3a), and RNAhybrid (v2.1.2). We identified overlapping genes across the three prediction tools. Filters of P < 0.05 and score > 0.5 were applied. Cytoscape software was used to construct the final interaction network.

Quantitative real-time PCR (qRT-PCR)

The QIAGEN exoRNeasy Serum Starter Kit (QIAGEN, Germany) extracted total exosomal RNA from human plasma samples. This procedure followed the manufacturer's protocol. The VAZYME HiScript II Q Select RT SuperMix kit (VAZYME, China) reverse-transcribed the purified RNA into cDNA. To eliminate genomic DNA contamination, we incubated the RNA preparations with gDNA Wiper Buffer at 42°C for 2 minutes. We then mixed the RNA template with miR-17-3p specific stem-loop primers and the reaction mixture. Incubation at 50°C for 15 minutes completed the reverse transcription. Quantitative real-time PCR determined miR-17-3p expression levels using SYBR Green chemistry. The total reaction volume was 10 μL. Each reaction mixed 2 μL of cDNA template with 0.2 μL each of forward and reverse primers. We also added 5 μL of ChamQ SYBR qPCR Master Mix, 0.2 μL of ROX reference dye, and 2.4 μL of RNase-free water. An initial denaturation step at 95°C for 10 minutes activated the enzyme. Amplification then proceeded through 40 cycles of 95°C for 15 seconds and 60°C for 60 seconds. A melting curve analysis verified the specificity of the amplified products. We analyzed all samples in triplicate. U6 small nuclear RNA served as the internal control. Finally, we calculated relative expression levels using the 2-ΔΔCt method. **Table 1** lists the specific primer sequences.

Statistical analysis

We performed all statistical analyses using SPSS 27.0 and GraphPad Prism 9.0. Frequencies and percentages [n (%)] represent categorical variables. To compare these categorical data, we utilized either the Pearson chi-square test or Fisher's exact test. The Shapiro-Wilk test evaluated the normality of continuous variables. Mean ± standard deviation

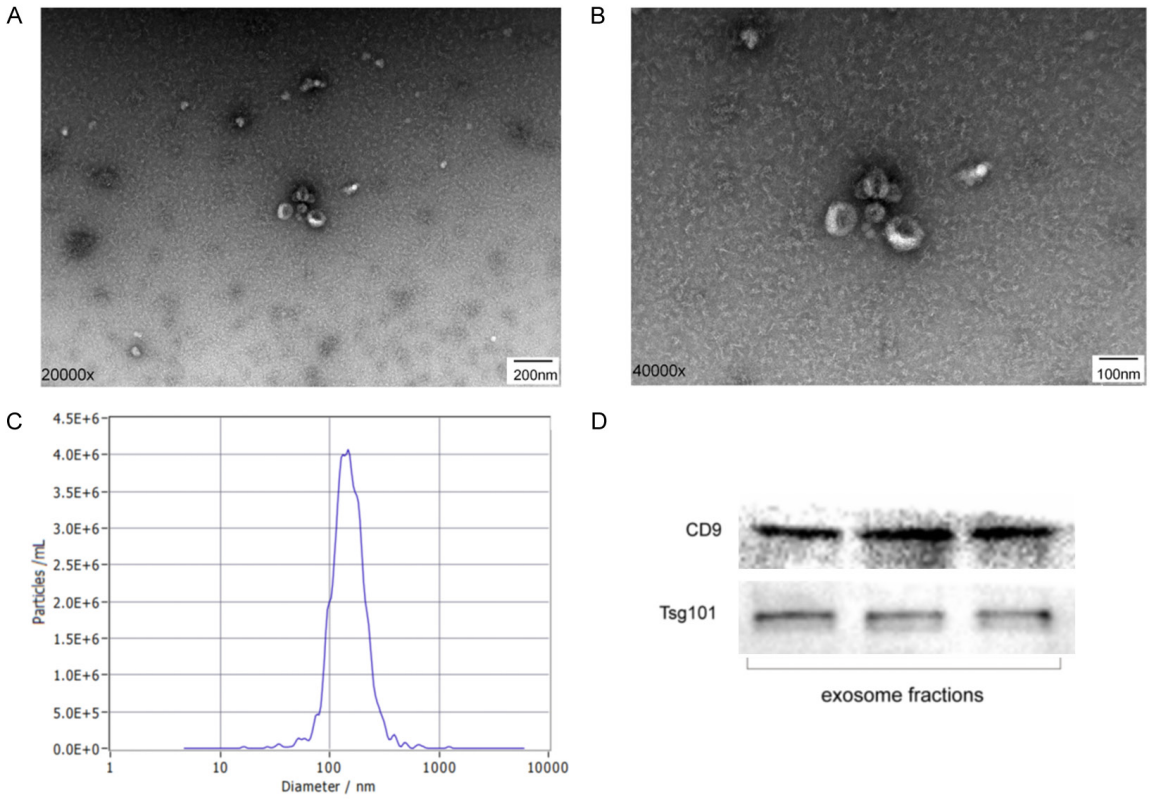

Figure 2. Identification and characterization of serum exosomes. A. Morphological characteristics of exosomes observed under transmission electron microscopy (scale = 200 nm, 20000×). B. Morphological characteristics of exosomes observed under transmission electron microscopy (scale = 100 nm, 40000×). C. Distribution of exosome particle size and concentration. D. Western blot analysis of exosomal marker proteins (CD9 and TSG101).

(Mean ± SD) expresses normally distributed data. Conversely, median and interquartile range (IQR) describe non-normally distributed datasets. For continuous variables, the independent-samples t-test analyzed normally distributed parameters. The Mann-Whitney U test evaluated non-normally distributed data. We established binary logistic regression models adjusting for age and sex. Adjusted predicted probabilities helped generate receiver operating characteristic (ROC) curves. We calculated the area under the curve (AUC) to assess diagnostic performance. A *P*-value < 0.05 determined statistical significance.

Results

Identification and characterization of serum exosomes

We successfully characterized serum exosomes through morphology, particle size, and protein markers. Transmission electron microscopy captured typical vesicle structures. These identified particles displayed round or irregular shapes. Nanoparticle tracking analysis using ZetaView yielded an average size of approximately 145.1 nm (**Figure 2A**, **2B**). The measured particle concentration reached roughly 6.5E+10 particles/mL (**Figure 2C**). Western blot analysis verified the clear presence of CD9 and TSG101 proteins (**Figure 2D**).

Small RNA profiling of serum exosomes

We performed high-throughput small RNA sequencing on serum exosomes from nine individuals. These participants included three healthy controls (Group N), three early-stage patients (Group T1), and three advanced-stage patients (Group T2). Across all groups, the detected miRNAs primarily spanned 20-22 nt in length. The 21 nt fragments exhibited the highest abundance (**Figure 3A-C**). PCA compared the global expression profiles among samples. In the principal component space, all

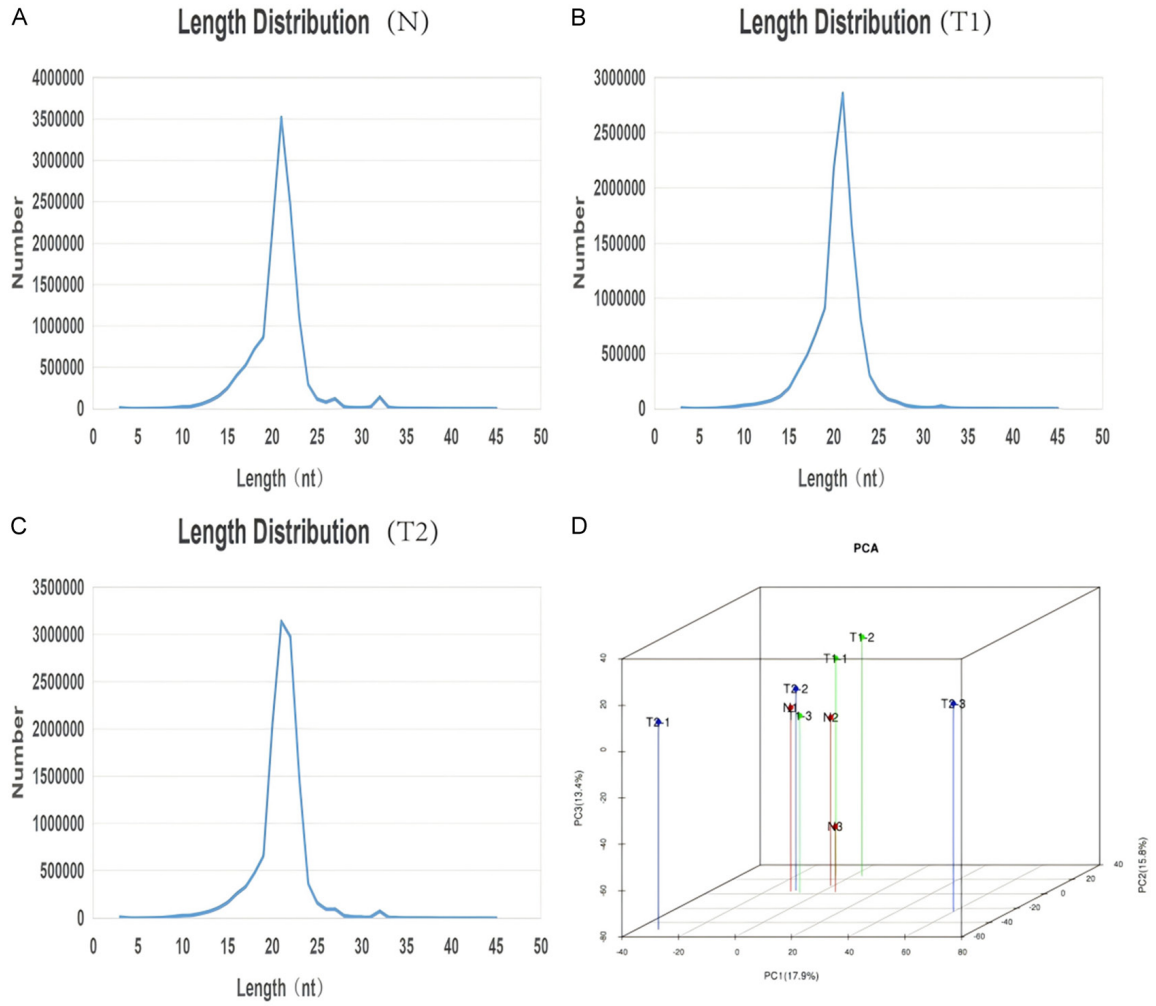

Figure 3. Small RNA profiling of serum exosomes. A. Length distribution of miRNAs in group N. B. Length distribution of miRNAs in group T1. C. Length distribution of miRNAs in group T2. D. Principal component analysis (PCA) of samples from groups N, T1, and T2. N: healthy individuals; T1: early-stage gastric cancer; T2: advanced gastric cancer.

samples overlapped without showing distinct clusters (**Figure 3D**). This overlap suggests consistent overall molecular characteristics across the cohorts.

Differential miRNAs expression profiles across gastric cancer stages

We screened differentially expressed miRNAs (DEMs) using a fold change ≥ 2 and statistical significance ($P < 0.05$) determined statistical significance. Scatter plots visualized these overall distribution trends (**Figure 4A-C**). Pairwise comparison between Group N and Group T1 identified 53 DEMs. Among these molecules, 11 showed downregulation, whereas 42 exhibited upregulation. Group N versus Group T2 comparisons revealed 28 DEMs. This subset comprised 18 downregulated and 10 upregulated miRNAs. We detected 40 DEMs between Group T1 and Group T2. This group included 30 downregulated and 10 upregulated miRNAs (**Figure 4D**). After further filtering for human-origin miRNAs, six DEMs (miR-10401-3p, miR-10b-5p, miR-222-5p, miR-324-5p, miR-4508, miR-642a-3p) were identified between Group N and Group T1 (**Figure 4E**); eight DEMs (miR-106b-3p, miR-11401, miR-1255b-5p, miR-132-3p, miR-17-3p, miR-451a, miR-616-3p, miR-6736-5p) between Group N and Group T2 (**Figure 4F**); and seven DEMs (miR-200a-3p, miR-204-3p, miR-3138, miR-4508, miR-574-5p, miR-615-3p, miR-6859-5p) between Group T1 and Group T2 (**Figure 4G**).

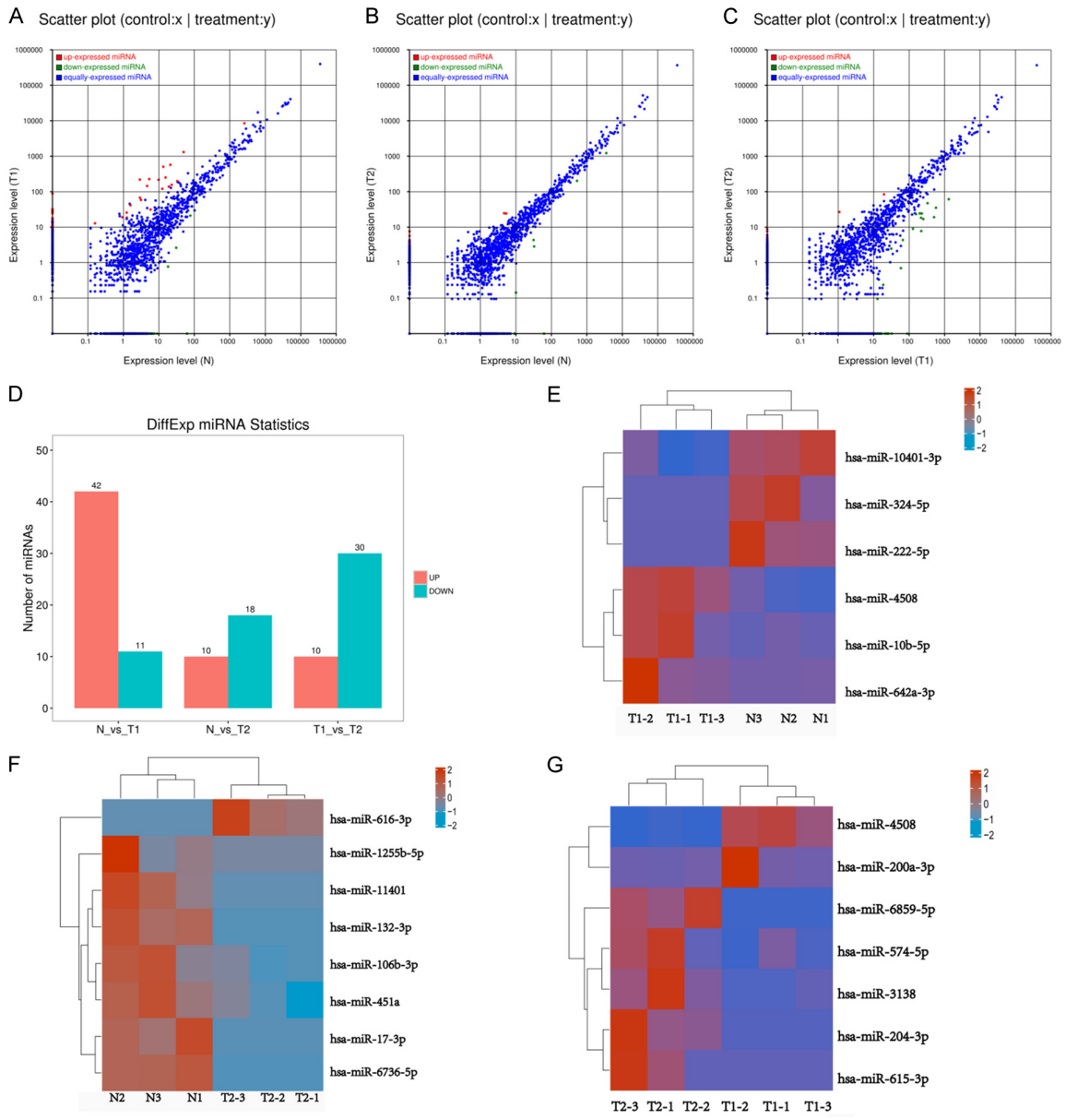

Figure 4. Differential miRNA expression profiles across gastric cancer stages. A. Scatter plot of differentially expressed miRNAs between N and T1. B. Scatter plot of differentially expressed miRNAs between N and T2. C. Scatter plot of differentially expressed miRNAs between T1 and T2. D. Bar chart of differentially expressed miRNAs among N, T1, and T2. E. Heatmap of human-derived differentially expressed miRNAs between N and T1. F. Heatmap of human-derived differentially expressed miRNAs between N and T2. G. Heatmap of human-derived differentially expressed miRNAs between T1 and T2.

These findings suggest that changes in specific miRNAs expression may be closely associated with gastric cancer progression (**Table 2**).

Dynamic classification and functional enrichment analysis of exosomal miRNAs

We classified differentially expressed exosomal miRNAs based on their dynamic expression patterns across tumor stages. This classification aimed to explore their potential roles in gastric cancer progression. The analysis divided all miRNAs into eight distinct trend modules (Profile 0-7). These modules contained 83, 848, 443, 251, 1066, 695, 193, and 50 miRNAs, respectively (**Figure 5A**). Profiles 0 and 7 exhibited clear unidirectional expression changes during gastric cancer evolution.

Table 2. Intergroup expression of differentially expressed miRNAs

Groups	miRNAs	TPM	TPM	Log2 (fc)	*P*-value
N vs T1		TPM (N)	TPM (T1)		
	miR-10401-3p	76.95	21.20	-1.86	0.0310
	miR-10b-5p	2573.81	8462.15	1.72	0.0498
	miR-222-5p	6.02	0.01	-9.23	0.0208
	miR-324-5p	8.85	0.01	-9.79	0.0062
	miR-4508	5.83	31.37	2.43	0.0356
	miR-642a-3p	0.94	18.98	4.34	0.0224
N vs T2		TPM (N)	TPM (T2)		
	miR-106b-3p	527.62	202.04	-1.38	0.0466
	miR-11401	5.99	0.01	-9.23	0.0045
	miR-1255b-5p	4.94	0.01	-8.95	0.0425
	miR-132-3p	4.46	0.01	-8.80	0.0121
	miR-17-3p	7.10	0.01	-9.47	0.0008
	miR-451a	3516.02	1221.32	-1.53	0.0130
	miR-616-3p	0.01	3.50	8.45	0.0273
	miR-6736-5p	3.29	0.01	-8.36	0.0377
T1 vs T2		TPM (T1)	TPM (T2)		
	miR-200a-3p	127.93	8.97	-3.83	0.0404
	miR-204-3p	0.01	4.68	8.87	0.0427
	miR-3138	1.08	26.78	4.63	0.0099
	miR-4508	31.37	2.48	-3.66	0.0091
	miR-574-5p	19.60	84.18	2.10	0.0482
	miR-615-3p	0.01	8.88	9.79	0.0234
	miR-6859-5p	0.01	5.02	8.97	0.0170

TPM: transcripts per million; N: healthy individuals; T1: early-stage gastric cancer; T2: advanced gastric cancer.

MiRNAs in Profile 0 decreased continuously. Conversely, those in Profile 7 displayed a persistently increasing trend. We then performed GO functional annotation and KEGG pathway enrichment analyses for these two modules. Profile 0 miRNAs primarily regulated cell junctions and cell adhesion processes. They also participated in MAPK, Wnt, VEGF, and ErbB signaling pathways (**Figure 5B**, **5C**). Profile 7 miRNAs significantly influenced actin cytoskeleton organization and focal adhesion formation. They also modulated cell adhesion processes. Multiple signaling cascades correlated with this module. These pathways included MAPK, Wnt, NF-κB, mTOR, Hippo, and AMPK (**Figure 5D**, **5E**).

Expression of miR-17-3p in gastric cancer and target gene prediction

Annotation and statistical analysis identified 36 human miRNAs in Profile 0. We also found 22 human miRNAs in Profile 7. Next, combined analysis based on fold change and significance narrowed down the candidates. This assessment revealed that miR-17-3p, miR-92a-3p, and miR-486-3p in Profile 0 decreased across gastric cancer stages. These changes reached statistical significance. Conversely, the 22 miRNAs in Profile 7 showed increasing expression trends. However, none achieved statistical significance (**Tables 3** and **4**). GO and KEGG enrichment analyses evaluated the biological roles of the three significant miRNAs. These molecules are primarily involved in cell development and differentiation. They also modulate intercellular signal transduction, cell adhesion, and proliferation. Furthermore, these miRNAs participate in multiple pathways closely related to gastric cancer development. Key cascades include the Gastric cancer, Hippo, mTOR, and PD-L1/PD-1 checkpoint pathways (**Figure 6A**, **6B**). Cytoscape software predicted the target genes of these differentially expressed miRNAs (**Figure 7**). Integrating the

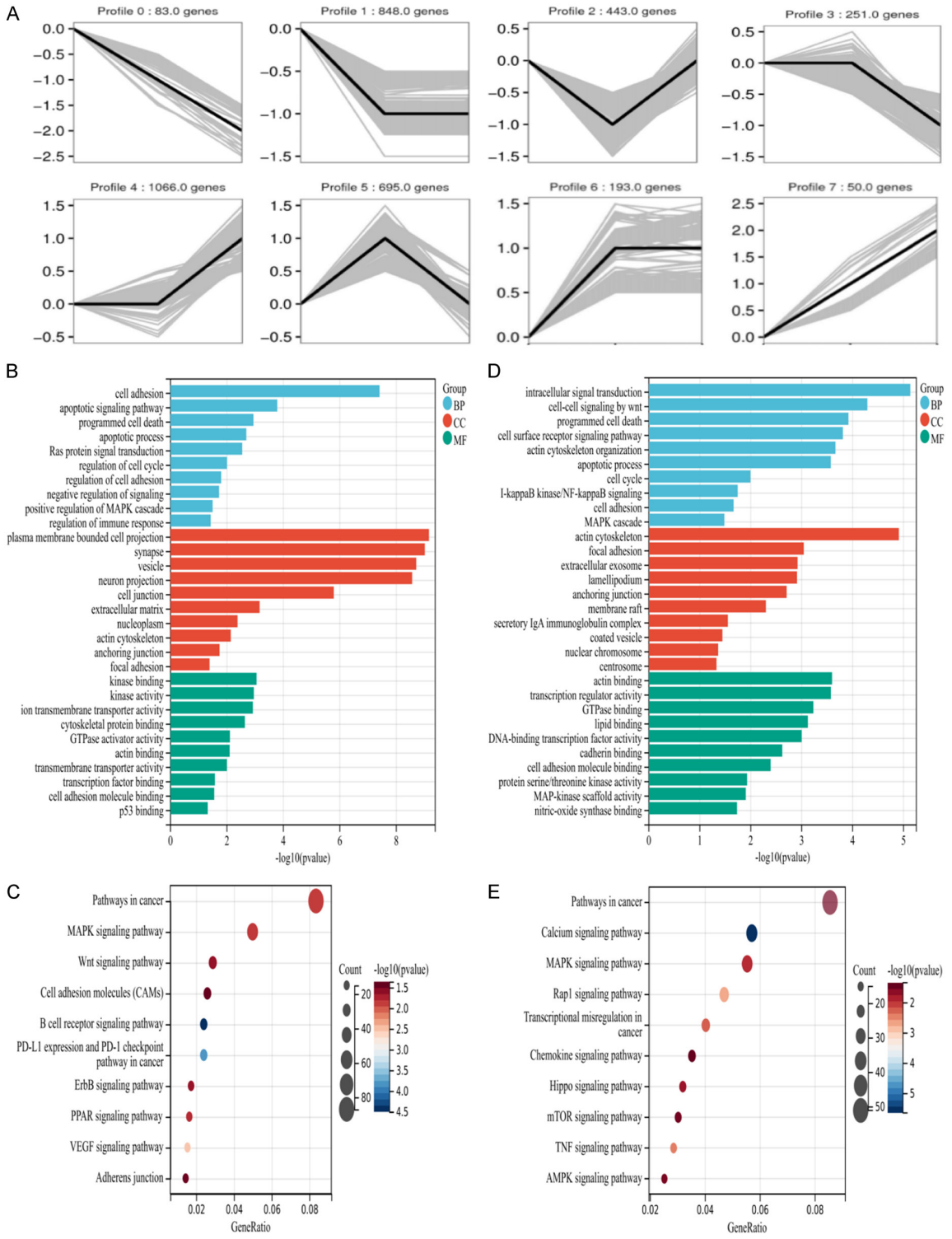

Figure 5. Dynamic classification and functional enrichment analysis of exosomal miRNAs. A. Expression trend of miRNAs in Profile 0-7 modules. B. GO annotation of miRNAs within the Profile 0 module. C. KEGG pathway enrichment analysis of miRNAs belonging to the Profile 0 module. D. GO functional annotation of miRNAs in the Profile 7 module. E. KEGG pathway enrichment analysis of miRNAs in the Profile 7 module. MF: Molecular Function; BP: Biological Process; CC: Cellular Component.

Table 3. Statistical list of differential miRNAs in the Profile 0 module

miRNAs	TPM (N)	TPM (T1)	TPM (T2)	Regulation	*P*-value
miR-10527-5p	4.18	2.19	1.59	Down	0.8821
miR-10b-3p	4.77	4.11	3.23	Down	0.9786
miR-128-3p	999.08	851.16	745.56	Down	0.8786
miR-144-5p	115.64	90.36	76.56	Down	0.4393
miR-151a-5p	22769.87	16078.18	12853.88	Down	0.5429
miR-16-5p	1444.03	1209.83	1117.14	Down	0.8286
miR-17-3p	**7.10**	**1.01**	**0.01**	**Down**	**0.0357**
miR-181c-3p	39.70	27.51	15.64	Down	0.2964
miR-182-5p	3337.23	2430.74	1960.65	Down	0.1964
miR-200c-3p	13.30	7.44	5.36	Down	0.1321
miR-2355-3p	2.87	2.01	1.20	Down	0.8929
miR-25-3p	3704.85	2845.62	2257.93	Down	0.2964
miR-30b-5p	166.33	106.81	82.80	Down	0.1679
miR-323a-5p	9.10	6.74	4.63	Down	0.4071
miR-326	10.15	2.01	0.95	Down	0.2286
miR-3928-3p	4.02	3.10	1.75	Down	0.7214
miR-423-5p	31892.26	26694.25	24642.82	Down	0.2321
miR-4485-3p	10.76	8.11	5.09	Down	0.5893
miR-4685-3p	13.73	9.97	6.59	Down	0.6286
miR-485-3p	61.60	39.37	24.49	Down	0.5107
miR-486-3p	**837.44**	**634.68**	**496.98**	**Down**	**0.025**
miR-505-5p	69.95	58.58	54.16	Down	0.6286
miR-5090	4.64	0.84	0.44	Down	0.2071
miR-532-5p	55.44	38.86	31.57	Down	0.1964
miR-548a-3p	1.24	0.16	0.01	Down	> 0.9999
miR-625-5p	6.82	3.95	2.55	Down	0.5714
miR-652-3p	68.20	38.40	29.95	Down	0.05
miR-6758-5p	1.83	1.34	0.67	Down	> 0.9999
miR-6777-5p	2.37	2.01	1.44	Down	> 0.9999
miR-6813-5p	4.26	0.32	0.01	Down	0.25
miR-6833-3p	1.35	0.51	0.33	Down	> 0.9999
miR-6837-3p	4.56	0.62	0.24	Down	0.5286
miR-92a-3p	**41867.35**	**29559.09**	**21451.38**	**Down**	**0.0286**
miR-93-3p	45.39	32.96	28.30	Down	0.1
miR-95-3p	5.58	4.08	2.67	Down	0.6786
miR-99b-3p	2.52	2.31	1.91	Down	0.8286

miRNAs in bold black are statistically significant.

differential analyses and expression trends, miR-17-3p, which showed a significant and progressive decrease in gastric cancer, was selected as a target molecule for subsequent research.

Diagnostic value of serum exosomal miR-17-3p in gastric cancer progression

We compared clinicopathological data between the early-stage (T1) and advanced-stage (T2) gastric cancer groups. Significant differences emerged in tumor diameter, differentiation degree, and lymph node invasion (**Table 5**). Nerve invasion, vascular tumor emboli, and TNM stage also varied significantly between groups ($P < 0.05$). Conversely, age and conventional serum markers (Carbohydrate Antigen 19-9, Carbohydrate Antigen 125, and Carcinoembryonic Antigen) showed no intergroup differences ($P > 0.05$). RT-PCR evaluated serum exosomal miR-17-3p expression. Its levels

Table 4. Statistical list of differential miRNAs in the Profile 7 module

miRNAs	TPM (N)	TPM (T1)	TPM (T2)	Regulation	*P*-value
miR-12136	0.01	0.16	4.35	Up	0.25
miR-1299	0.64	1.70	3.20	Up	0.5714
miR-152-3p	328.19	339.30	353.05	Up	0.9286
miR-32-5p	5.94	7.37	8.21	Up	0.4393
miR-382-5p	41.12	52.06	59.93	Up	0.2536
miR-432-5p	128.72	148.72	196.69	Up	0.6286
miR-4467	1.84	2.71	4.48	Up	0.6786
miR-450a-5p	8.29	9.67	11.48	Up	0.9286
miR-4659a-3p	4.75	5.31	5.68	Up	0.9857
miR-4667-5p	2.42	3.02	3.69	Up	0.8071
miR-4677-3p	2.18	2.40	2.53	Up	> 0.9999
miR-493-5p	6.10	11.14	14.19	Up	0.7214
miR-494-3p	22.82	25.68	34.29	Up	0.7214
miR-504-5p	4.32	5.00	6.76	Up	0.7929
miR-548j-5p	0.23	0.55	1.76	Up	0.4643
miR-576-3p	0.96	1.84	2.45	Up	0.6786
miR-6511a-3p	20.73	22.93	25.66	Up	0.9286
miR-6716-3p	0.56	1.09	2.49	Up	> 0.9999
miR-6772-3p	2.43	2.71	3.20	Up	> 0.9999
miR-6802-3p	0.42	0.93	2.25	Up	> 0.9999
miR-937-3p	1.51	1.78	2.25	Up	0.9571
miR-939-5p	1.25	2.40	4.26	Up	0.6679

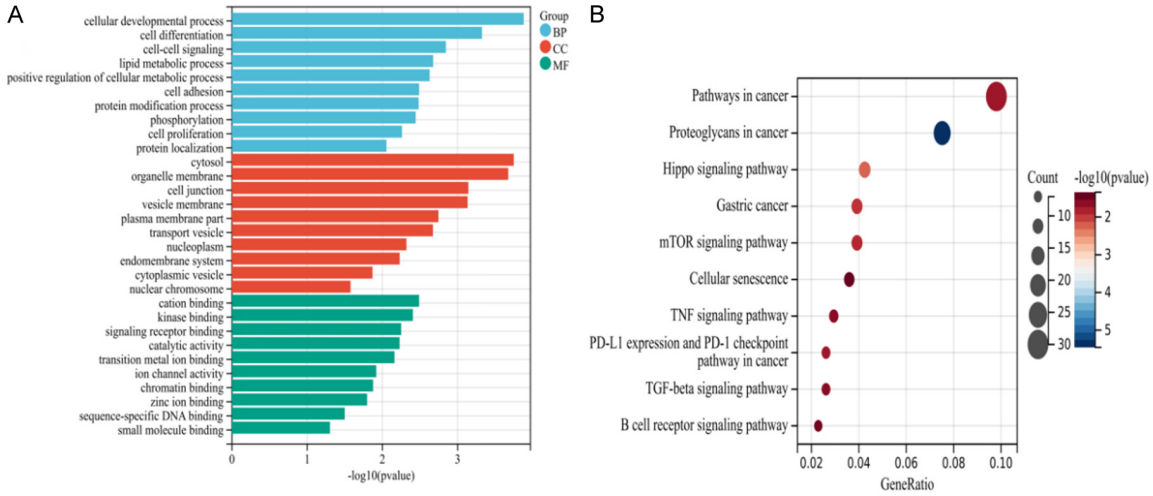

Figure 6. GO functional annotation and KEGG pathway enrichment analysis of miR-17-3p, miR-486-3p, and miR-92a-3p. A. GO functional annotation. B. KEGG pathway enrichment analysis.

showed a stepwise decrease across the healthy control, T1, and T2 groups (P < 0.05, **Figure 8A**). Stratified analysis indicated that miR-17-3p expression correlated with tumor differentiation (P = 0.0324). This molecule also correlated with TNM stage (P = 0.0100) and nerve invasion (P = 0.0100, **Table 6**). After adjusting for age and sex, we established logistic regression models to predict the progression of GC. These models generated boxplots and ROC curves. We evaluated three diagnostic models to distinguish advanced GC from early-stage

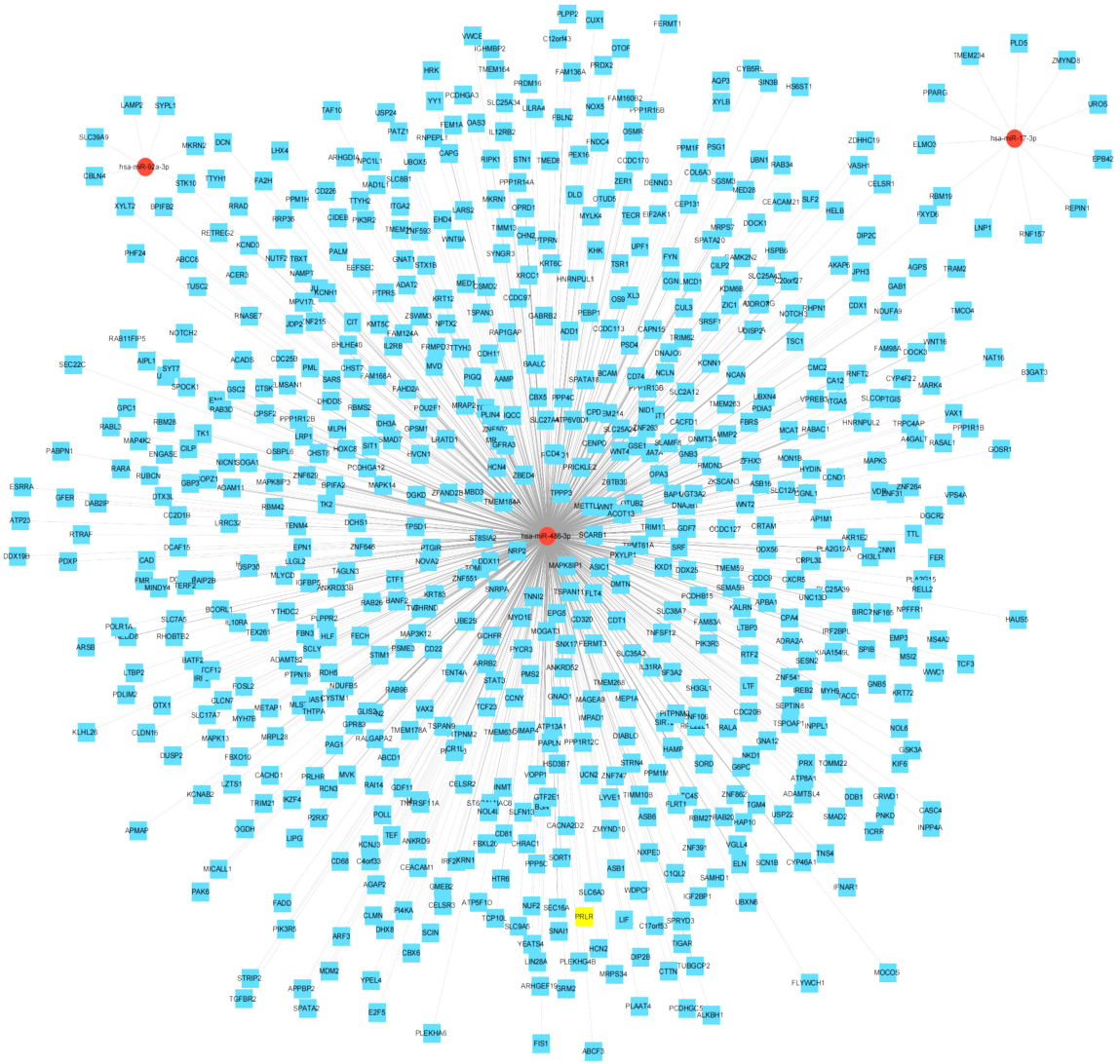

Figure 7. Target gene prediction of miR-17-3p, miR-486-3p, and miR-92a-3p.

disease. Individual or combined parameters all demonstrated strong predictive power ($P < 0.05$, **Figure 8B-D**). Specifically, miR-17-3p alone yielded an AUC of 0.8403 (**Figure 8E**). The conventional marker panel produced a lower AUC of 0.7847 (**Figure 8F**). Ultimately, integrating miR-17-3p with conventional markers achieved the highest AUC of 0.8472 ($P < 0.01$, **Figure 8G**).

Discussion

Gastric cancer ranks among the most prevalent digestive system malignancies worldwide. This disease drives exceptionally high global incidence and mortality rates. Typically, early-stage gastric cancer develops without obvious or specific clinical manifestations. Many patients are not diagnosed until the disease reaches an advanced stage or metastasizes to distant organs [14]. Therefore, identifying sensitive and specific non-invasive biomarkers holds profound clinical importance.

Clinicians widely use conventional serum tumor markers for malignancy diagnosis. These common markers include CEA, CA19-9, and CA-125. In GC, tumor cells secrete these molecules or induce their expression. Their serum levels correlate closely with invasion depth and metastatic status [15]. The high-molecular-weight glycoprotein CA-125 serves as an important indicator for monitoring tumor recurrence. However, GC detection yields a positi-

Table 5. Clinical data of early-stage gastric cancer and advanced-stage gastric cancer

Clinical Parameter	T1	T2	*P*-value
Age (years)	64.83±6.617	66.42±8.426	0.6138
Maximum tumor diameter (cm)	2.258±1.082	5.608±3.290	0.0004
Sex			0.0361
Male	10 (83.33%)	4 (33.33%)	
Female	2 (16.67%)	8 (66.67%)	
Tumor differentiation degree			0.0013
Well/moderate	8 (66.67%)	0	
Moderate-low/poor	4 (33.33%)	12 (100.00%)	
Lymph node invasion			0.0001
Yes	1 (8.33%)	11 (91.67%)	
No	11 (91.67%)	1 (8.33%)	
TNM stage			< 0.0001
0-I	12 (100.00%)	0	
II-III	0	12 (100.00%)	
Nerve invasion			< 0.0001
Yes	0	12 (100.00%)	
No	12 (100.00%)	0	
Vascular tumor emboli			0.0006
Yes	2 (16.67%)	11 (91.67%)	
No	10 (83.33%)	1 (8.33%)	
Tumor markers (U/mL or ng/mL)			
CA-199	13.78±10.57	33.08±51.96	0.1277
CA-125	14.26±10.55	18.44±17.57	0.4428
CEA	2.598±1.738	2.523±1.517	0.8428

CA-199: carbohydrate antigen 199; CA-125: carbohydrate antigen 125; CEA: carcinoembryonic antigen.

vity rate of only 41.2% for this marker [16]. CEA participates directly in cell adhesion mechanisms. Tumors upregulate CEA during growth and distant metastasis. Yet, its diagnostic sensitivity for GC reaches merely 58.4% [17]. Additionally, CA19-9 expression correlates positively with TNM stage and lymph node metastasis. Inflammatory conditions like pancreatitis and cholangitis also elevate CA19-9 levels [18-20]. This overlap drives a higher false-positive rate. Although these markers remain useful for preoperative assessment, their serum levels lack sufficient specificity and sensitivity. They demonstrate notable limitations in differentiating early from advanced GC.

MicroRNAs (miRNAs) exhibit excellent stability in bodily fluids like blood and saliva. Clinicians can readily obtain these molecules via non-invasive methods. Prior research indicates that miRNAs participate extensively in proliferation, differentiation, and programmed cell death. Through these cellular activities, they directly influence tumor initiation and progression [5]. Recently, bioinformatics approaches leveraging multi-omics data predicted several abnormal miRNA profiles in gastric cancer tissues. These candidates include miR-2681-3p, miR-6807-3p, miR-6499-5p, and miR-379-3p [21]. Their altered expression level correlates significantly with patient prognosis. Such findings position miRNAs as promising molecular markers for prognostic evaluation. They may also serve as novel therapeutic intervention targets for gastric cancer patients.

Exosomal cargo comprises diverse non-coding RNAs, including miRNAs, circular RNAs, and long non-coding RNAs. These encapsulated molecules maintain high stability under physiological conditions. Crucially, exosomes reflect the real-time physiological and pathological status of their parental cells. These vesicles represent a primary focus in tumor liquid biopsy research. Multiple clinical studies have highlighted their diagnostic relevance in malignant

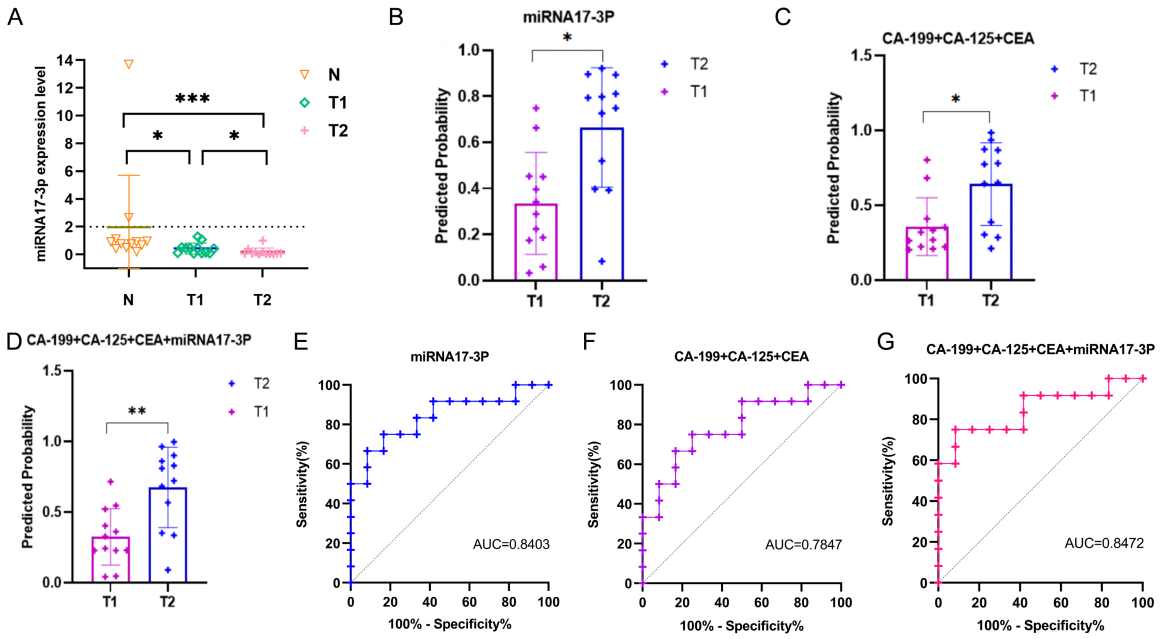

Figure 8. Diagnostic value of serum exosomal miR-17-3p in gastric cancer progression. A. Expression levels of miR-17-3p among groups N, T1, and T2. B. The predictive probability of miR-17-3p for groups T1 and T2. C. The predictive probability of the combined panel of CA19-9, CA-125 and CEA for groups T1 and T2. D. The predictive probability of the combined panel of miR-17-3p, CA19-9, CA-125 and CEA for groups T1 and T2. E. ROC curves of miR-17-3p for groups T1 and T2. F. ROC curves of the combined panel of CA19-9, CA-125, and CEA for groups T1 and T2. G. ROC curves of the combined panel of miR-17-3p, CA19-9, CA-125 and CEA for groups T1 and T2. ROC: Receiver operating characteristic. AUC: The area under the curve. $*P < 0.05$; $**P < 0.01$; $***P < 0.001$.

tumors. Ren et al. [22] reported elevated serum exosomal hsa-let7f-5p levels in patients with metastatic pancreatic cancer. This miRNA may contribute to metastasis by regulating proteins such as high-mobility group protein AT-hook 2. Chen et al. [23] reported upregulation of serum exosomal lncRNA-DLEU1 in cervical cancer. Compared with squamous cell carcinoma antigen or CA-125, it achieved higher specificity (86.0%) and sensitivity (61.4%). Another report demonstrated that plasma exosomal circLPAR1 was significantly downregulated in gastric cancer patients. Reduced expression correlated with poor differentiation, and vascular invasion [24]. This study analyzed the dynamic evolution of exosomal miRNA expression profiles across three clinical groups. Serum exosomal small RNA sequencing profiled healthy volunteers alongside early-stage and advanced gastric cancer patients. Through this approach, we identified miR-17-3p. We subsequently provided a preliminary validation of its clinical utility. Combining miR-17-3p with CA19-9, CA-125, and CEA significantly enhanced diagnostic performance.

The purified exosomes matched established criteria for morphology, size distribution, and positive marker protein expression. Sequence length analysis revealed a predominant size of 21 nucleotides for small RNAs across all sample groups. This length represents a hallmark feature of mature miRNAs. PCA demonstrated a gradual shift in overall expression profiles across the experimental groups. This pattern suggests continuous changes in exosomal miRNA expression during gastric cancer progression. Differential expression analysis revealed unique miRNA signatures for early-stage and advanced gastric cancer. Specifically, we identified 53 differentially expressed miRNAs between Group N and Group T1. In contrast, 28 differentially expressed miRNAs occurred between Group N and Group T2. This difference indicates more extensive miRNA dysregulation during early-stage gastric cancer development. Trend analysis subsequently grouped the differentially expressed miRNAs into eight distinct clusters. Among these, Profile 0 and Profile 7 exhibited unidirectional progressive trends. Functional annotation linked Profile 0

Table 6. Relationship between miR-17-3p and clinicopathological characteristics in different stages of gastric cancer

Clinical parameter	Number of cases	MiR-17-3p	
		Mean (± SD)	*P*-value
Sex			0.1915
Male	14	0.3995±0.4295	
Female	10	0.1920±0.1793	
Age (years)			0.2598
≤ 60	7	0.1446±0.1289	
> 60	17	0.3824±0.3999	
Maximum tumor diameter (cm)			0.1829
≤ 5	19	0.3560±0.3855	
> 5	5	0.1498±0.1542	
Tumor differentiation degree			0.0324
Well/moderate	8	0.5120±0.4514	
Moderate-low/poor	16	0.2136±0.2630	
Lymph node metastasis			0.1135
Yes	12	0.2243±0.2900	
No	12	0.4018±0.4073	
TNM stage			0.0100
0-I	12	0.4394±0.3939	
II-III	12	0.1867±0.2778	
Nerve invasion			0.0100
Yes	12	0.1867±0.2778	
No	12	0.4394±0.3939	
Vascular tumor emboli			0.2284
Yes	13	0.2420±0.2847	
No	11	0.3971±0.4269	

miRNAs primarily to cell junction and adhesion. These molecules also target canonical signaling pathways including MAPK and Wnt. Crucially, the MAPK pathway modulates tumor cell proliferation, differentiation, and apoptosis. And Wnt signaling actively drives tumorigenesis [25, 26]. Sustained downregulation of Profile 0 miRNAs potentially overactivates these identified pathways. This molecular event drives early-stage gastric cancer initiation and progression. Meanwhile, Profile 7 miRNAs regulate actin cytoskeleton remodeling and focal adhesion formation. Dynamic cytoskeleton remodeling gives tumor cells the necessary structural basis for migration and invasion. And concurrent aberrant focal adhesion formation coordinates extracellular matrix degradation and metastatic lesion development [27, 28]. Moreover, Profile 7 miRNAs modulate several critical signaling cascades. These targets encompass the mTOR, NF-κB, and Hippo pathways. Such cascades heavily dictate tumor proliferation, tissue invasion, and inflammatory responses. Our findings suggest that these miRNAs may contribute to gastric cancer progression. They may facilitate the transition from localized tumor growth to an invasive phenotype.

The miR-17 family includes both miR-17-3p and miR-17-5p. Post-transcriptional processing generates these two mature strands from a single precursor, pre-miR-17 [29]. Yet, some evidence highlights their divergent behavior. These two mature miRNAs exhibit distinct expression patterns across different malignancies. Prior studies consistently demonstrate miR-17-5p upregulation in gastric and colorectal cancers. Knockdown of this molecule effectively inhibits tumor cell proliferation, invasion, and migration [30, 31]. Several reports identified elevated miR-17-3p levels in tumor tissues or serum samples from patients with colorectal cancer and thyroid cancer [32, 33]. But Shincy et al. [34] identified the miR-17-3p might play a tumor suppressor role in breast cancer through bioinformatics analysis. And Bourogianni et al. [35] detected higher serum miR-17-3p expression in benign thyroid nodules than in papillary thyroid carcinoma. These findings suggest that the expression of miR-17-3p in body fluids may be influenced by multiple factors, including tumor type and disease progression. Current literature predominantly explores the biological role of miR-17-5p in gastrointestinal tumors. Conversely, researchers have rarely investigated serum exosomal miR-17-3p in gastric cancer. Its exact relationship with gastric malignancy progression remains poorly understood. Systematic evaluations of its clinical utility are still lacking. Serum exosomal miR-17-3p levels decreased stepwise during gastric cancer progression. Healthy individuals, early-stage patients, and advanced-stage patients exhibited distinct expression profiles. This stage-related pattern implies a potential regulatory role for miR-17-3p in tumor development. Clinicopa-

thological analysis further showed that lower miR-17-3p levels were closely linked with tumor differentiation, TNM stage, and nerve invasion. For distinguishing early from advanced gastric cancer, single miR-17-3p yielded an AUC of 0.8403. This score demonstrates strong discriminatory power. Conversely, the traditional marker model produced an AUC of only 0.7847. Integrating miR-17-3p with traditional markers elevated the diagnostic AUC to 0.8472. These findings suggest that serum exosomal miR-17-3p distinguishes gastric cancer across different progression stages. Combining this molecule with conventional tumor markers further enhances staging accuracy. Nevertheless, the present study contains notable limitations. The validation cohort exceeded the discovery cohort in size. Yet, the overall sample size remained relatively small. Future multicenter investigations with larger cohorts must further validate these preliminary results.

Conclusion

In summary, this study systematically revealed dynamic changes in serum exosomal miRNAs during gastric cancer progression. Exosomal miR-17-3p expression levels demonstrate strong value for distinguishing different disease stages. Moreover, we combined miR-17-3p with conventional markers, including CA19-9, CA-125, and CEA. This integrated panel markedly enhances diagnostic capacity for staging gastric cancer.

Acknowledgements

We appreciate every author for their assistance with the experiments and constructive comments on the manuscript. We would like to thank the anonymous reviewers for their constructive comments. The study received research grants from Science and Technology Program Project of Jiangxi Provincial Health Commission (202310237); and Jiangxi Provincial Natural Science Foundation (20252BAC240445).

Written informed consent was obtained from the patients or guardians.

Disclosure of conflict of interest

None.

Address correspondence to: Junfu Wang, Department of General Surgery, The First Affiliated Hospital, Jiangxi Medical College, Nanchang University, No. 17 Yongwai Zheng Street, Nanchang 330006, Jiangxi, China. E-mail: ndyfy09538@ncu.edu.cn

References

[1] Bray F, Laversanne M, Sung H, Ferlay J, Siegel RL, Soerjomataram I and Jemal A. Global cancer statistics 2022: GLOBOCAN estimates of incidence and mortality worldwide for 36 cancers in 185 countries. CA Cancer J Clin 2024; 74: 229-263.

[2] Siegel RL, Miller KD and Jemal A. Cancer statistics, 2020. CA Cancer J Clin 2020; 70: 7-30.

[3] Morgan E, Arnold M, Camargo MC, Gini A, Kunzmann AT, Matsuda T, Meheus F, Verhoeven RHA, Vignat J, Laversanne M, Ferlay J and Soerjomataram I. The current and future incidence and mortality of gastric cancer in 185 countries, 2020-40: a population-based modelling study. EClinicalMedicine 2022; 47: 101404.

[4] Necula L, Matei L, Dragu D, Neagu AI, Mambet C, Nedeianu S, Bleotu C, Diaconu CC and Chivu-Economescu M. Recent advances in gastric cancer early diagnosis. World J Gastroenterol 2019; 25: 2029-2044.

[5] Jelski W and Mroczko B. Molecular and circulating biomarkers of gastric cancer. Int J Mol Sci 2022; 23: 7588.

[6] Fu M, Gu J, Jiang P, Qian H, Xu W and Zhang X. Exosomes in gastric cancer: roles, mechanisms, and applications. Mol Cancer 2019; 18: 41.

[7] Conti CB, Agnesi S, Scaravaglio M, Masseria P, Dinelli ME, Oldani M and Uggeri F. Early gastric cancer: update on prevention, diagnosis and treatment. Int J Environ Res Public Health 2023; 20: 2149.

[8] Mori MA, Ludwig RG, Garcia-Martin R, Brandão BB and Kahn CR. Extracellular miRNAs: from biomarkers to mediators of physiology and disease. Cell Metab 2019; 30: 656-673.

[9] Coenen-Stass AML, Pauwels MJ, Hanson B, Martin Perez C, Conceição M, Wood MJA, Mäger I and Roberts TC. Extracellular microRNAs exhibit sequence-dependent stability and cellular release kinetics. RNA Biol 2019; 16: 696-706.

[10] Wan M, Ning B, Spiegel S, Lyon CJ and Hu TY. Tumor-derived exosomes (TDEs): how to avoid the sting in the tail. Med Res Rev 2020; 40: 385-412.

[11] Zhang C, Yang J, Chen Y, Jiang F, Liao H, Liu X, Wang Y, Kong G, Zhang X, Li J, Gao J and Shen L. miRNAs derived from plasma small extracel-

lular vesicles predict organo-tropic metastasis of gastric cancer. Gastric Cancer 2022; 25: 360-374.
[12] Wu L, Zhang X, Zhang B, Shi H, Yuan X, Sun Y, Pan Z, Qian H and Xu W. Exosomes derived from gastric cancer cells activate NF-κB pathway in macrophages to promote cancer progression. Tumour Biol 2016; 37: 12169-12180.
[13] Zhang Y, Han T, Feng D, Li J, Wu M, Peng X, Wang B, Zhan X and Fu P. Screening of non-invasive miRNA biomarker candidates for metastasis of gastric cancer by small RNA sequencing of plasma exosomes. Carcinogenesis 2020; 41: 582-590.
[14] Huang Y, Shao Y, Yu X, Chen C, Guo J and Ye G. Global progress and future prospects of early gastric cancer screening. J Cancer 2024; 15: 3045-3064.
[15] Xiao ML, Fu L, Ma FH, Li YA, Zhang GF and Qiang JW. Comparison of MRI features among squamous cell carcinoma, adenocarcinoma and adenosquamous carcinoma, usual-type endocervical adenocarcinoma and gastric adenocarcinoma of cervix. Magn Reson Imaging 2024; 112: 10-17.
[16] Streppel MM, Vincent A, Mukherjee R, Campbell NR, Chen SH, Konstantopoulos K, Goggins MG, Van Seuningen I, Maitra A and Montgomery EA. Mucin 16 (cancer antigen 125) expression in human tissues and cell lines and correlation with clinical outcome in adenocarcinomas of the pancreas, esophagus, stomach, and colon. Hum Pathol 2012; 43: 1755-1763.
[17] He CZ, Zhang KH, Li Q, Liu XH, Hong Y and Lv NH. Combined use of AFP, CEA, CA125 and CAI9-9 improves the sensitivity for the diagnosis of gastric cancer. BMC Gastroenterol 2013; 13: 87.
[18] Liu X, Cai H and Wang Y. Prognostic significance of tumour markers in Chinese patients with gastric cancer. ANZ J Surg 2014; 84: 448-453.
[19] Su SB, Qin SY, Chen W, Luo W and Jiang HX. Carbohydrate antigen 19-9 for differential diagnosis of pancreatic carcinoma and chronic pancreatitis. World J Gastroenterol 2015; 21: 4323-4333.
[20] Wannhoff A, Brune M, Knierim J, Weiss KH, Rupp C and Gotthardt DN. Longitudinal analysis of CA19-9 reveals individualised normal range and early changes before development of biliary tract cancer in patients with primary sclerosing cholangitis. Aliment Pharmacol Ther 2019; 49: 769-778.
[21] Qian H, Cui N, Zhou Q and Zhang S. Identification of miRNA biomarkers for stomach adenocarcinoma. BMC Bioinformatics 2022; 23: 181.
[22] Ren S, Song LN, Zhao R, Tian Y and Wang ZQ. Serum exosomal hsa-let-7f-5p: a potential diagnostic biomarker for metastatic pancreatic cancer detection. World J Gastroenterol 2025; 31: 109500.
[23] Chen Y, Cui F, Wu X, Zhao W and Xia Q. The expression and clinical significance of serum exosomal-long non-coding RNA DLEU1 in patients with cervical cancer. Ann Med 2025; 57: 2442537.
[24] Yang X, Xia J, Peng C and Cai W. Expression of plasma exosomal circLPAR1 in patients with gastric cancer and its clinical application value. Am J Cancer Res 2023; 13: 4269-4276.
[25] Kadasah SF. Targeting the MAPK pathway in cancer. Int J Mol Sci 2025; 27: 214.
[26] Lee J, Kim S, Oh Y, Jahn SR, Kim J, Kim Y, Schmäche T, Kim SM, Teriyapirom I, Groß T, Kwon O, Kim J, Kim S, Ada AM, Català-Bordes A, Cho Y, Kim J, Andersson-Rolf A, Merker SR, Lim JY, Park JY, Klompstra TM, Yoon KJ, Lim DS, Lee HS, Kim JK, Choi E, Goldenring JR, Cheong JH, Kim H, Stange DE, Lee H, Koo BK and Lee JH. Epithelial WNT secretion drives niche escape of developing gastric cancer. Mol Cancer 2025; 25: 1.
[27] Lechuga S, Amin PH, Wolen AR and Ivanov AI. Adducins inhibit lung cancer cell migration through mechanisms involving regulation of cell-matrix adhesion and cadherin-11 expression. Biochim Biophys Acta Mol Cell Res 2019; 1866: 395-408.
[28] Narasimhan BN and Fraley SI. Matrix degradation enhances stress relaxation, regulating cell adhesion and spreading. Proc Natl Acad Sci U S A 2025; 122: e2416771122.
[29] Yang X, Du WW, Li H, Liu F, Khorshidi A, Rutnam ZJ and Yang BB. Both mature miR-17-5p and passenger strand miR-17-3p target TIMP3 and induce prostate tumor growth and invasion. Nucleic Acids Res 2013; 41: 9688-9704.
[30] Chen P, Zhao H, Huang J, Yan X, Zhang Y and Gao Y. MicroRNA-17-5p promotes gastric cancer proliferation, migration and invasion by directly targeting early growth response 2. Am J Cancer Res 2016; 6: 2010-2020.
[31] Liu Z, Ji M, Jin F, Jiang F and Liu X. Expression and clinical significance of miR-17-5p in tumor tissues of patients with colorectal cancer. J Gastrointest Oncol 2022; 13: 3067-3079.
[32] Ng EK, Chong WW, Jin H, Lam EK, Shin VY, Yu J, Poon TC, Ng SS and Sung JJ. Differential expression of microRNAs in plasma of patients with colorectal cancer: a potential marker for colorectal cancer screening. Gut 2009; 58: 1375-1381.

[33] Takakura S, Mitsutake N, Nakashima M, Namba H, Saenko VA, Rogounovitch TI, Nakazawa Y, Hayashi T, Ohtsuru A and Yamashita S. Oncogenic role of miR-17-92 cluster in anaplastic thyroid cancer cells. Cancer Sci 2008; 99: 1147-1154.

[34] Shincy JS, Panagal M, Jereena J, Vengatagiri GY, Vittalrao KR, Sivakumar P, Gopinath V, Kumar KM and Sekar D. Computational identification of microRNA-17-3p in breast cancer cells. Microrna 2017; 6: 208-212.

[35] Bourogianni O, Tsitoura E, Sifakis K, Kapsoritakis N, Karatzanis A, Doulaptsi M, Antoniou K, Koukouraki S and Prokopakis E. Disease-relevant preoperative serum miRNA levels in papillary thyroid cancer. Biology (Basel) 2026; 15: 626.